small
NANO MICRO

Self-Propelled Activated Carbon Janus Micromotors for Efficient Water Purification

*Beatriz Jurado-Sánchez, Sirilak Sattayasamitsathit, Wei Gao, Luis Santos, Yuri Fedorak, Virendra V. Singh, Jahir Orozco, Michael Galarnyk, and Joseph Wang**

Self-propelled activated carbon-based Janus particle micromotors that display efficient locomotion in environmental matrices and offer effective 'on-the-fly' removal of wide range of organic and inorganic pollutants are described. The new bubble-propelled activated carbon Janus micromotors rely on the asymmetric deposition of a catalytic Pt patch on the surface of activated carbon microspheres. The rough surface of the activated carbon microsphere substrate results in a microporous Pt structure to provide a highly catalytic layer, which leads to an effective bubble evolution and propulsion at remarkable speeds of over 500 μm/s. Such coupling of the high adsorption capacity of carbon nanoadsorbents with the rapid movement of these catalytic Janus micromotors, along with the corresponding fluid dynamics and mixing, results in a highly efficient moving adsorption platform and a greatly accelerated water purification. The adsorption kinetics and adsorption isotherms have been investigated. The remarkable decontamination efficiency of self-propelled activated carbon-based Janus micromotors is illustrated towards the rapid removal of heavy metals, nitroaromatic explosives, organophosphorous nerve agents and azo-dye compounds, indicating considerable promise for diverse environmental, defense, and public health applications.

1. Introduction

Self-propelled catalytic nanomotors, capable of converting energy into movement and forces, have shown considerable promise for diverse practical applications.[1–10] While initial efforts have focused on biomedical applications of nano/microscale motors,[11–13] recent activity has illustrated their potential for variety of environmental applications.[14,15] In particular, microscale machines have been shown to add a new dimension based on motion to decontamination processes and to lead to new 'on-the-fly' remediation protocols, with higher efficiency, shorter cleanup time and potentially lower costs.[14,15] The continuous movement of such microscale objects can be used for transporting reactive (water-purification) nanomaterials throughout contaminated samples,[16] for releasing and dispersing remediation agents over long distances,[17,18] and for imparting significant mixing during decontamination processes (without external forced convection, *e.g.*, stirring).[19] For example, our group illustrated the use of superhydrophobic alkanethiol-coated tubular microengines and seawater-driven Janus micromotors for effective removal of oil droplets,[20,21] and the use of micromotors for accelerated oxidative detoxification of organophosphorus nerve agents.[19] Sanchez and coworkers reported the use of rolled-up tubular microengines comprising of a reactive material (Fe) for degrading organic pollutants in water *via* the Fenton oxidation process.[16] New micromachines, capable of removing a wide range of contaminants from polluted water, could have major impacts upon public safety.[14,15]

Dr. B. Jurado-Sánchez, Dr. S. Sattayasamitsathit, Dr. W. Gao, Dr. L. Santos, Y. Fedorak, Dr. V. V. Singh, Dr. J. Orozco, M. Galarnyk, Prof. J. Wang
Department of Nanoengineering
University of California
San Diego, La Jolla CA 92093, USA
E-mail: josephwang@ucsd.edu

DOI: 10.1002/smll.201402215

Herein, we combine the remarkable adsorption capacity of activated carbon microspheres with the dynamic movement of Janus micromotors for creating highly efficient moving adsorption platforms. Activated carbons have been the most common and cost-effective nano/microscale adsorbents for the removal of a wide range of pollutants from aquatic media, owing to their high specific surface area, short intraparticle diffusion distance, and tunable pore size, and surface chemistry.[22–28] The Safe Drinking Water Act Amendments of 1986 have identified granular activated carbon as the best technology for removing organic contaminants from water supplies. These nanoadsorbents have been shown to be extremely useful for the removal of a wide range of organic[26–28] and inorganic pollutants.[29,30] For example, activated carbon microparticles can remove toxic heavy metals via electrostatic attraction to various oxygen-containing surface groups or organic compounds by dispersive interactions or hydrogen bonding.[28]

In the following sections we will discuss the development and characterization of catalytic activated carbon Janus particles micromotors and will demonstrate their highly efficient self-propulsion and remarkable water decontamination efficiency (**Figure 1**A). The adsorption properties of activated carbon microparticles are thus combined with an attractive propulsion performance and enhanced fluid dynamics and mixing to offer *'on-the-fly'* accelerated water purification processes. Unlike these early nanomotor-based decontamination efforts involving the movement or release of reactive remediation agents, the new activated carbon micromotors can universally remove and isolate broad range of chemicals (without decomposing them).

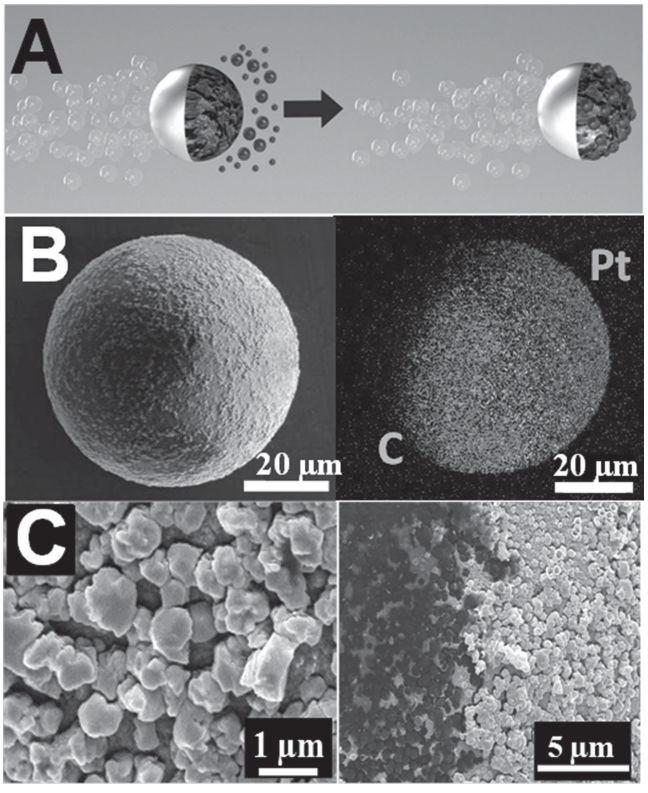

Figure 1. (A) Schematic of the activated carbon/Pt Janus micromotor and its 'on-the-fly' decontamination use. The dark hemisphere (right) represents the spherical activated carbon, while the grey area (left) corresponds to the catalytic Pt hemisphere patch. (B) Scanning electron microscope (SEM, left) image and energy-dispersive X-ray (EDX, right) spectroscopy images illustrating the distribution of carbon (C) and Pt in the Janus micromotor. (C) SEM images of the rough Pt catalytic layer (left) and of the activated carbon/Pt interface of the Janus micromotors (right).

2. Results and Discussion

Figure 1A shows the schematic of the activated carbon based Janus micromotor and of the corresponding 'on-the-fly' water decontamination. The new micromotors were prepared using commercially-available carbon microparticles (Supel™Sphere carbon) possessing a remarkably high surface area (100 m^2/g) and micropore density. These characteristics have played a dual role in the present study, by leading to extremely fast adsorption kinetics and to efficient propulsion of the resulting mobile adsorption platforms. To obtain such autonomous propulsion, these activated carbon particles have been sputter-coated with a 60 nm thick catalytic Pt hemispheric layer. The new micromotors have an average diameter of 60 μm and can propel at a fast speed of 550 ± 120 μm/s, corresponding to a relative speed of nearly 10 body lengths/s. Such fast movement in the presence of chemical fuel reflects the net momentum associated with the detachment of oxygen microbubbles from the catalytic Pt patch, which leads to a directional propulsion thrust.

Scanning electron microscopy (SEM) and energy dispersive X-ray spectroscopy (EDX) analyses have been used for characterizing the surface of the activated carbon/Pt Janus micromotors. Figure 1B illustrates the spherical morphology of the Janus micromotor (diameter ~60 μm). The EDX and SEM data also indicate that the microparticle has a distinct binary structure, with a thick platinum film—coating half of the activated carbon sphere—forming the catalytic Janus micromotor. The SEM images of Figure 1C illustrate that the resulting Pt layer displays a very rough morphology, compared to common Janus particles.[31] Such close examination of the catalytic Pt patch reveals that the Pt surface is composed of granular metal microparticles with an average diameter of ~0.8 μm which leads to a dramatically increased catalytic surface area and to an improved movement behavior.[32–34]

The rough catalytic surface promotes effective bubble evolution and propulsion. For example, the microscopic images in **Figure 2**A,a, taken from SI Video 1, illustrate the movement of the activated carbon/Pt Janus micromotor in pure water over a 4 sec period. A long high-density tail of oxygen microbubbles (~5 μm in diameter) is generated and ejected from the platinum surface. The fast bubble generation frequency and the steady motor propulsion are also clearly illustrated in the corresponding video. The effective propulsion reflects the continuous thrust of oxygen bubbles generated by the spontaneous catalytic reaction of the peroxide fuel. The Janus micromotor is self-propelled at an ultrafast speed of over 550 ± 120 μm/s. This speed corresponds to a very large drive force of over 300 pN, based on

small 2014,
DOI: 10.1002/smll.201402215

NANO MICRO small

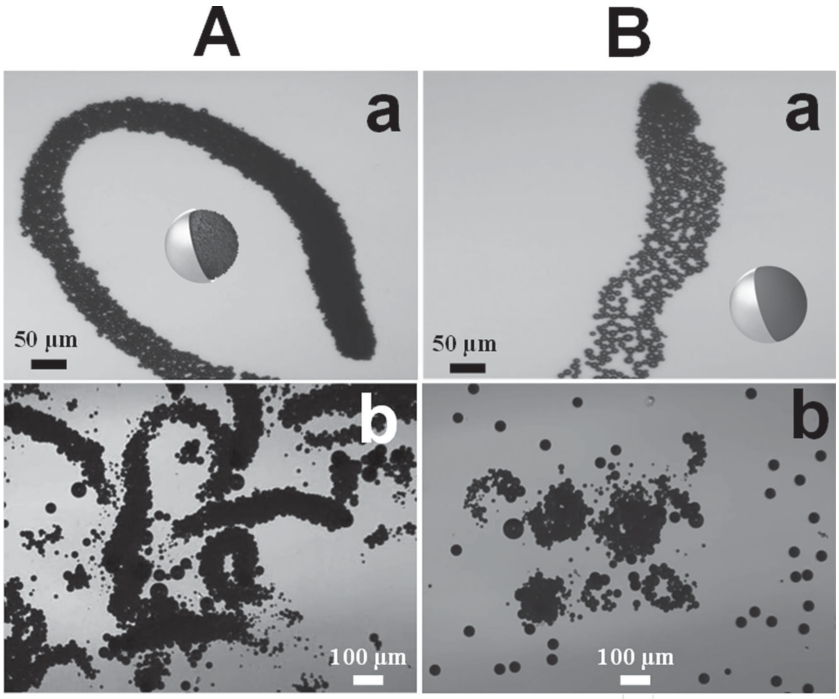

Figure 2. Efficient propulsion of the activated carbon/Pt microsphere Janus motors. (A) Time-lapse images illustrating the motors propulsion over a 4 sec period, as compared with (B) control (PS)/Pt microparticles in (a) ultrapure water (taken from SI video 1) and (b) 70% seawater (taken from SI video 2). Media: ultrapure water or seawater (a and b, respectively) containing 10% H_2O_2 and 2% sodium cholate.

the drag force for a spherical colloid (equals the drive force), $F = 6\pi\mu av$, where a is the radius of the sphere, v is the speed of the micromotor, and μ is the viscosity of water. Such high speed is highly stable which is essential for practical environmental applications. As expected, the speed of the activated carbon/Pt Janus micromotors is strongly dependent on the peroxide fuel concentration (Figure S1). The speed increases from 190 ± 65 μm/s to 350 ± 85 μm/s and 550 ± 120 μm/s using 2, 6, and 10% fuel, respectively. Control experiments were also conducted using polystyrene (PS)/Pt Janus micromotors (of similar size but a smooth catalytic surface), in order to examine the role of the substrate and resulting Pt layer in the higher propulsion thrust and speed. Under similar conditions, the (PS)/Pt micromotors display a greatly slower speed of 300 ± 60 μm/s, along with larger bubble size and a lower bubble density reflecting the slower bubble generation rate (see Figure 2B, a and Video S1). Apparently, the microporous structure of the catalytic Pt layer of the activated carbon-Janus micromotor strongly affects the nucleation, pinning, and growth of the oxygen bubbles, leading to higher bubble production rate compared to traditional Janus motors (A vs. B; Figure 2a).

The new activated carbon-based Janus micromotor can operate in real-life environmental matrices. The images in Figure 2A,b and the corresponding SI Video S2 illustrate the efficient movement of multiple activated carbon/Pt micromotors in a 70% seawater samples at a high speed of 350 μm/s ± 70 (~6 body lengths/s). The slower speed of the micromotors in this media, compared to pure water (550 μm/s ± 120 μm/s), reflects the higher viscosity of seawater and the presence of co-existing molecules that can partially passivate the catalytic Pt surface.[35] The trajectory of the micromotors was not altered by the seawater matrix. In contrast, only about 15% of the common polystyrene/Pt Janus micromotors display movement in the seawater sample and at a dramatically lower speed of 55 μm/s ± 13 μm/s (Figure 2B, b and SI Video 2). Apparently, the microporous Pt surface and the corresponding bubble thrust of the activated carbon based Janus micromotors facilitate their rapid movement in seawater samples, compared to the polystyrene Janus micromotor. Such repeated movement of multiple activated carbon/Pt micromotors across the contaminated samples, along with the high-density tail of microbubbles, results in a greatly enhanced mass transport (without external agitation), and leads to a higher water purification efficiency using significantly shorter times when compared to the use of static activated carbon particles.

To demonstrate the practical decontamination capability of the new activated carbon/Pt micromotors, associated with their movement and resulting mixing, we examined their ability to remove a broad spectrum of pollutants of organic (nerve agents, explosives, dyes) and inorganic (heavy metals) nature. Experiments were performed by immersing a suspension of the motors (10^6 motors/mL) in 0.5 mL samples containing various levels of the different target pollutants. The motors were propelled in the contaminated solution for 5 min in the presence of 2% H_2O_2 fuel. **Figure 3**A and B demonstrate the efficient micromotor-induced removal of 2,4-dinitrotoluene (DNT) and lead, respectively. In both cases, a dramatic decrease of the contaminant electrochemical response, corresponding to over 90% removal, is observed following the treatment with the activated carbon based micromotors (line 1). In contrast, only a negligible removal (~1–5%) of these pollutants is observed in control experiments carried out using the uncoated activated carbon microparticles (line 3) or polystyrene-based Pt Janus micromotors (line 2). These data indicate that the new dynamic adsorption platforms offer significantly shorter remediation times and the motor movement is crucial for such accelerated decontamination process. To further investigate the crucial role of the motor movement, control experiments were carried out by immersing the micromotors in contaminated solutions but in the absence of the hydrogen peroxide fuel. This study indicated a negligible (~1–5%) removal of all the same pollutants (not shown). Another control experiment was carried out in the presence of 2% of the peroxide fuel but without the micromotors. This experiment resulted in no apparent change in pollutant levels, indicating that this fuel level has no effect upon the stability of all the pollutants examined.

We have also investigated the influence of the number of micromotors upon the adsorptive removal of different

DOI: 10.1002/smll.201402215

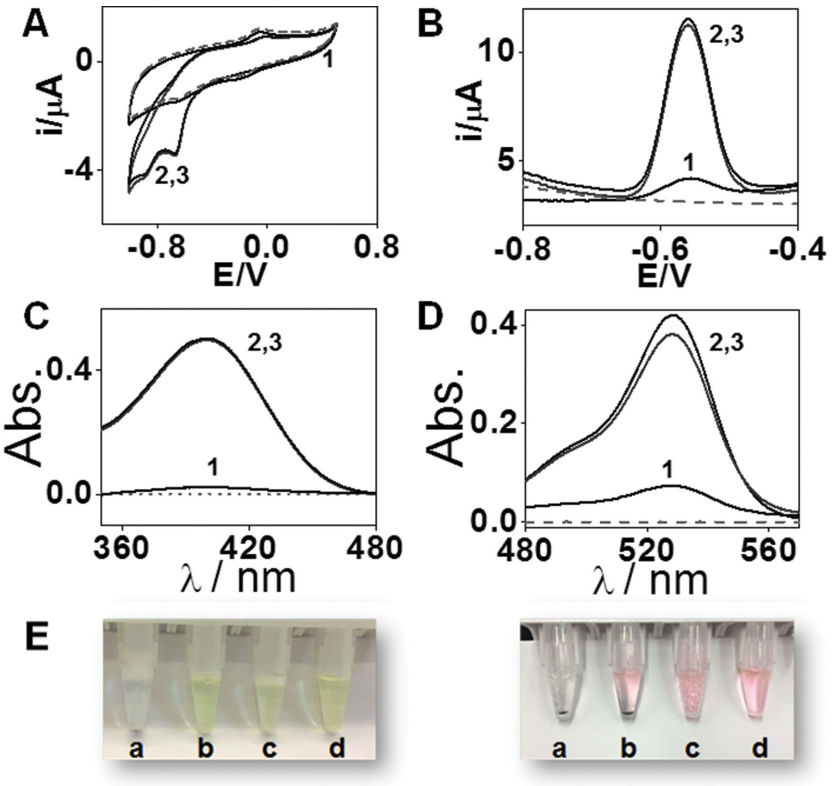

Figure 3. Removal of different pollutants from aqueous solutions using self-propelled activated carbon/Pt micromotors along with control experiments using uncoated activated carbon particles and polystyrene-based Pt Janus micromotors: (A) Cyclic voltammograms for 2,4-dinitrotoluene (DNT, C_0 = 100 mg/L); (B) Stripping voltammograms of Pb^{2+} (C_0 = 2 mg/L); (C) Absorbance spectra of the p-NP product of methyl-paraoxon (C_0 = 100 μM); and (D) absorbance spectra of Rhodamine 6G (C_0 = 4 mg/L) after 5 min treatment with activated carbon/Pt micromotors (line 1) uncoated activated carbon particles (line 3) and Janus (PS)/Pt motors (line 2). Dotted lines represent the blank signal. (E) Photographs of a solution polluted with 100 μmol of methyl-paraoxon and (F) 4 mg/L of Rhodamine 6G after 5 min treatment with (a) the activated-carbon/Pt micromotors (b) non-sputtered activated-carbon particles and (c) (PS)/Pt motors, as compared with the initial conditions (d). Conditions: 2% H_2O_2, and 10^6 micromotors or activated carbon particles in a total volume of 0.5 mL. 2% sodium cholate and 2% sodium dodecyl sulphate were used as surfactant in experiments with DNT or Pb^{2+}, methyl-paraoxon or Rhodamine 6G, respectively.

levels of DNT and lead from aqueous media. As illustrated in Figure S2, higher levels of both pollutants are removed upon increasing the motor density (from 52 to 96% DNT or from 51 to 90% Pb, upon increasing the number of motors from 2 to 10 × 10^5 micromotors/mL, respectively). To expand the practical utility of the activated carbon/Pt based micromotors towards diverse environmental applications, we examined their ability to remove the nerve agent simulant methyl-paraoxon and to decolorize a dye (Rhodamine 6G) contaminated solution (Figure 3C and D, respectively). The sharp decrease in the absorbance signal of the *p*-nitrophenol hydrolysis product of the remaining methyl-paraoxon in solution (C, line 1) and of Rhodamine 6G (D, line 1) following the motor treatment demonstrates the effectiveness moving the activated carbon platform for the adsorption of both compounds, with percent removals higher than 92%. In contrast, negligible elimination is observed in the control experiments with uncoated (static) activated carbon particles and polystyrene-based Pt Janus micromotors (lines 2 and 3, respectively). This data was supported by the rapid (5 min) discoloration of highly colored contaminated solution of methyl-paraoxon and Rhodamine 6G using the activated carbon/Pt motors, as compared with the intense color observed in control experiments using the static unmodified activated carbon microparticles, or the (polysterene)/Pt microsphere motors, along with the initial conditions (before using activated carbon motors) (not shown). A negligible removal was also observed in these control experiments even after a longer 60 min treatment. Overall, these data emphasize the importance of combining the adsorption capacity of activated carbon particles with their dynamic movement for an accelerated water purification and that the motor movement is crucial for the fast, efficient removal of pollutants.

The adsorption behavior of the activated carbon/Pt Janus micromotor has been analyzed by applying Langmuir and Freundlich adsorption isotherm models,[36] using methyl-paraoxon and lead as the model organic and inorganic species, respectively. Details of this study are described in the experimental section. The Freundlich model is given by the following equation:

$$\ln q_e = \ln K_f - \frac{1}{n}\ln C_e$$

The linear form of the Langmuir equation is represented by the following equation:

$$\frac{1}{q_e} = \frac{1}{Q} + \frac{1}{Q_b C_e}$$

Where q_e is the amount of adsorption at the equilibrium (mg/g) (after 5 min treatment with the activated carbon/Pt micromotors), C_e is the equilibrium concentration (mg/l), of the target pollutant, and K_f (adsorption capacity of adsorbent) and n (favorability of adsorption process) are Freundlich constants. Q_b is the amount of solute adsorbed per unit weight of adsorbent in forming a complete monolayer on the surface and *b* is a constant related to the energy or net enthalpy. The applicability of the experimental data to isotherm models was examined. Figure S3A shows the Freundlich adsorption isotherm for methyl-paraoxon (a) and Pb^{2+} (b) on the activated carbon-based Janus micromotors. The linear plot of ln q_e *vs.* ln C_e suggests that both pollutants conform to the Freundlich isotherm model, with correlation coefficients (R^2) higher than 0.900. The *n* values, calculated from the slope of each calibration graph, were found to be

small 2014,
DOI: 10.1002/smll.201402215

NANO MICRO small

1.19 and 2.64 for methyl-paraoxon and $Pb^{2+,}$ respectively, indicating that the adsorption of both compounds is a favorable physical process.[29] The adsorption data, however, does not fit well with the Langmuir isotherm model, as indicated by the low correlation coefficients obtained for both methyl-paraoxon (Figure S3B, a) and Pb^{2+} (Figure S3B, b). In addition, the negative value for the Langmuir constant b obtained in the case of methyl-paraoxon indicates that this model is inadequate for describing the adsorption behavior of the Janus micromotor, since the constant represents the surface binding energy.

Figure 4A compares the decontamination rate of 100 μM of methyl-paraoxon (a) or 2 mg/L of lead (b) under different conditions. As expected, negligible (<5%) removal is observed over the entire 5 min period in control experiments involving moving PS/Pt micromotors (blue line) or stationary uncoated activated carbon particles (red line). In contrast, the presence of the activated carbon motors results in a rapid removal of these model pollutants (black line). About 60% methyl-paraoxon and 85% lead are thus removed within the first minute, and over 90% over the entire 5 min. The kinetics of methyl-paraoxon and Pb^{2+} adsorption was also investigated using two different models: the pseudo-first order and pseudo-second order kinetics. The procedures of kinetic experiments were basically identical to those of the adsorption isotherms studies (see experimental section). The adsorption rate constants were first determined from the pseudo first-order equation:[36]

$$\ln(q_e - q_t) = \ln q_e - k_1 t$$

where q_e and q_t are the amount of pollutant absorbed at the equilibrium and at a time t (sec) and k_1 is the rate constant of the first order (min^{-1}). The results obtained are listed in Table S1.This Table shows that the correlation coefficients are higher than 0.800 in some cases; the calculated q_e values do not fit with the experimental q_e values (obtained from the linear plots), indicating that the adsorption of methyl-paraxon and Pb^{2+} onto the moving activated carbon micromotor is not a first-order kinetic. On the other hand, the second-order adsorption rate equation is expressed as:

$$\frac{1}{q_t} = \frac{1}{k_2 q_e^2} + \left(\frac{1}{q_t}\right) t$$

If second-order kinetics is applicable, the plot of *t/q* versus *t* should show a linear relationship. The linear plot of *t/q* versus *t* (Figure 4B,a and B,b for methyl-paraoxon and Pb^{2+}, respectively) displays a good agreement between the experimental and calculated *qe* values (Table S1). The R2 values for the second-order kinetic model range from 0.982 to 0.998 (Table S1), indicating the applicability of this equation and the second-order nature of the adsorption process on activated carbon Janus micromotors. Table S1 shows also that the *k2* values decrease upon increasing the pollutant concentration, indicating a lower sorption kinetics at higher pollutant concentration.

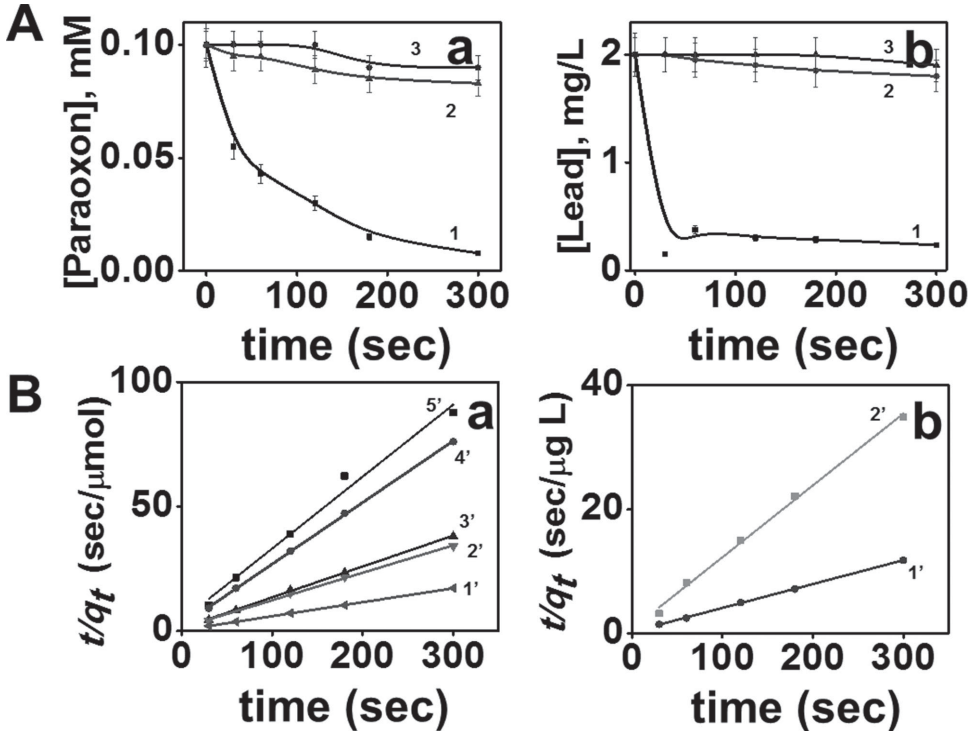

Figure 4. (A) Time dependence of the removal of 100 μM of methyl-paraoxon (a) or 2 mg/L of lead (b) using activated carbon/Pt Janus motor (black line), (PS)/Pt micromotors (blue line) or uncoated activated carbon particles (red line). (B) Pseudo-second-order kinetic model for removal of methyl-paraoxon (a) and lead (b) by activated carbon/Pt micromotors, at different concentrations: 750 (line 5′), 1000 (line 4′), 1500 (line 3′), 2000 (line 2′) and 3000 μM (line 1′) for methyl-paraoxon and 2000 (line 2′, b) and 5000 μg/L (line 1′, b) for Pb^{2+}.

DOI: 10.1002/smll.201402215

3. Conclusions

We have described the preparation and behavior of Janus micromotors based on activated carbon microparticles. The new micromotors combine the remarkable adsorption capacity of activated carbon microspheres with highly efficient bubble propulsion in natural water samples. The improved propulsion performance has been attributed to the microporous Pt surface (on the rough carbon substrate) that offers a greatly enhanced catalytic activity and efficient bubble evolution compared with common Janus micromotors. Accordingly, the new activated carbon based micromotors can operate efficiently in raw viscous real-life environmental media and maintain high speeds in such samples.

The continuous movement of multiple activated carbon/Pt micromotors across, along with the high-density tail of microbubbles, results in a greatly enhanced fluid dynamics that leads to a significantly higher water purification efficiency and short cleanup times compared to static activated carbon particles. These newly developed Janus micromotors can reach large areas of a contaminated sample accelerating the decontamination process without external mixing force. The remarkable decontamination power of the new activated carbon micromotor has been demonstrated in connection to a variety of model organic and inorganic pollutants. Kinetic models and Langmuir and Freundlich adsorption isotherm models have been used to characterize the efficient adsorption processes. These advances add a new dimension to recent motor-based decontamination protocols based on the removal (and not decomposition) of target chemicals. Such 'on-the-fly' adsorptive pickup can thus be used for enriching the collected targets. These new developments are expected to advance rapidly into practical environmental applications. While peroxide-driven motors are used here for proof-of-concept of the self-propelled activated carbon 'moving-filters', and peroxide can be readily decompose to water and oxygen,[16] many practical environmental applications of the new moving activated carbon devices—particularly in-situ ones—would require the use of alternative (environmentally-friendly) fuels. In particular, recently introduced water-based micromotors[21] would allow to move the activated carbon 'filters' using the water sample itself as an in-situ fuel. Alternately, the concept can be applied using fuel-free micromotors (based on ultrasound or magnetic propulsions).

4. Experimental Section

Synthesis of Activated Carbon/Janus Motors: The spherical activated carbon/Janus motors were prepared using Supel Sphere carbon particles (60 μm, Sigma-Aldrich, USA) as the base particles. Carbon particles were cleaned in distilled water and subsequently filtered through a 5 μm filter membrane. 60 μL of the particles were dispersed in isopropanol, which were then spread onto the glass slides and dried under room temperature. The particles were coated with a 60 nm Pt layer using a Denton Discovery 18 unit. The deposition was performed at room temperature with a DC power of 200 W and an Ar pressure of 2.5 mT for 60 s. In order to obtain a uniform Janus half-shell coating, rotation was turned off and the sample slides were set up at an angle to be parallel to the Pt target. After the fabrication, the Janus activated carbon/Pt particles were pipette off from the substrate and kept in deionizer water. The control Janus particles were prepared using polystyrene (PS) microparticles (45 μm mean diameter, Polysciences Inc., USA) as the base particles. A 60 μL aliquot of the PS-particles solution was spread onto glass slides and dried uniformly to form particle monolayers. The sputtering steps were the same as for the fabrication of the activated carbon Janus particles. Control activated carbon particles, without Pt coating, were examined for pollutant adsorption.

Propulsion of Janus Motor: The propulsion of Janus micromotors was tested. A known volume of the solution containing the Janus motors was dropped on a glass slide, followed by an equal volume of a solution of surfactant and the same volume of hydrogen peroxide fuel, to get a final concentration of 2% sodium cholate (or 1% sodium dodecyl sulfate) and 10% H_2O_2. An inverted optical microscope (Nikon Eclipse Instrument Inc. Ti-S/L100), coupled with a 4X objective, a Hamamatsu digital camera C11440 and NIS Elements AR 3.2 software, were used for capturing movies at a rate of 45 frames per sec. The speed of the micromotors was tracked using a NIS Elements tracking module.

Electrochemical Measurement of 2,4-Dinitrotoluene and Lead: All electrochemical measurements were performed using an Autolab PGSTAT 12 (Eco Chemie, The Netherlands). Glassy carbon electrode (GCE) and platinum and Ag/AgCl (1 M KCl) electrodes were employed as a working, counter and reference electrode, respectively. For, DNT measurement, the GCE was polished using 3–4 μm Al_2O_3 powder then rinsed with ultrapure water followed by immerging GCE in acetonitrile for 5 min. The electrochemical reduction and oxidation of the 2,4-dinitrotoluene (DNT) was characterized using cyclic voltammetric technique. The potential was swept from +0.5 V to −1.0 V at scan rate 100 mV s^{-1}. CVs were scanned until the stabilized signals were obtained. Ultrapure water was used to prepare all solutions. 2,4-DNT stock solution was prepared daily in acetonitrile (10 g/L), and working solutions were prepared by dilution of this stock in double distilled water. All electrochemical measurements were carried out using a 50 mM phosphate buffer solution (PBS, pH 6.5) as electrolyte. Oxygen was removed from the solution before each measurement by purging with N_2 gas. The voltammetric signals for DNT were recorded using 10 to 200 mg/L levels. The removal of DNT was examined by taking 100 μL aliquots of the solution, which were added into 2 mL PBS:acetonitrile (1:1) electrochemical cell. The removal of heavy metals was evaluated using anodic-stripping voltammetry, which was accomplished using GCE, platinum and Ag/AgCl (1 M KCl) electrodes. The GCE was polished using 3–4 μm Al_2O_3 powder then rinsed with ultrapure water. The electrode was subsequently immersed in 1 M HNO_3 for 5 min to ensure the removal of metal contamination. A 0.1 M acetate buffer solution (ABS) was used as an electrolyte. Pb^{2+} (10 mg/L) and Bi^{2+} stock solutions were prepared in doubled distilled water. Stripping voltammetric measurements were performed with an in situ deposition of a bismuth film and Pb^{2+} in the presence of dissolved oxygen. Measurements were completed by adding 25 μL sample aliquots into a 5 mL electrochemical cell, containing 0.1 M ABS buffer and 400 μg/L of bismuth, and controlling constant magnetic stirring at 1000 rpm. A deposition potential of −1.2 V was applied for 10 min to the carbon working electrode, while

small 2014,
DOI: 10.1002/smll.201402215

the solution was stirred for plating lead and bismuth. The stripping voltammogram was recorded by applying a positive-going square-wave voltammetric potential scan from −1.2 to 0.0 V (with a frequency of 20 Hz, amplitude of 25 mV, and potential step of 5 mV). A 30-s conditioning step at +0.3 V (with solution stirring) was used to remove the Pb^{2+} and bismuth followed by electrode polishing prior to the next cycle.

Spectrophotometric Measurement of Methyl-paraoxon and Rhodamine 6G: All measurements were performed with a UV-Vis spectrophotometer (UV-2450, SHIMADZU) equipped with a constant temperature circulating bath. For methyl-paraoxon, absorption curves were determined by monitoring the quantitative appearance of *p*-NP at 400 nm, a product of its basic hydrolysis (with 1.5 M NaOH). Rhodamine 6G concentration was determined by measuring the absorbance at 524 nm. Stock solutions (50 mM for methyl-paraoxon and 1 g/L for Rhodamine 6G) were prepared daily in double distilled water and subsequently diluted to the required concentration.

Freundlich and Langmuir Isotherms: Adsorption isotherms studies were carried with five different initial concentrations of methyl-paraoxon (750, 1000, 1500, 2000 and 3000 μM) or Pb^{2+} (2000, 3000, 4000, 5000 and 6000 μg/L) while maintaining a fixed number of motors (10^6 motors/mL) and 2% H_2O_2 fuel concentration in 0.5 mL solutions. The motors were navigated for 5 min in each solution, allowing sufficient time to reach the adsorption equilibrium. The study was performed at room temperature to be representative of environmentally relevant conditions. All experiments were carried out in duplicate under identical conditions and the average value was used for further calculation. The amount of adsorption at equilibrium, q_e, was calculated by:

$$q_e = \frac{(C_0 - C_e)}{m}$$

where C_0 and C_e are the liquid-phase concentrations of *methyl*-paraoxon or Pb^{2+} at initial and equilibrium, respectively. V is the volume of the solution and m is the mass of Janus micromotors used. The Janus micromotors' weight was calculated to be 2.359 g/cm^3 by drying a measured sample of known particle concentration. Due to a variety in particle radii, an average of volume and surface area was established by analyzing the microscope images of approximately 1000 particles by using ImageJ program for data analysis. Spherical particle radii were used to calculate individual weight, which was averaged over the entire sampled specimen equaling 5.75×10^{-7} g/particle.

Pseudo First Order and Pseudo Second Order Kinetics: Kinetics studies were carried using five different initial concentrations of methyl-paraoxon (750, 1000, 1500, 2000 and 3000 μM) or Pb^{2+} (2000, 3000, 4000, 5000 and 6000 μg/L), while maintaining a fixed number of motors (10×10^5 motors/mL) in 0.5 mL solutions containing 2% H_2O_2 and 2% sodium dodecyl sulphate. Samples were collected at preselected time intervals (30, 60, 120, 180 and 300 s), and the concentrations of methyl-paraoxon and Pb^{2+} were measured. The amount of adsorption at time t, qt was calculated by:

$$q_e = \frac{(C_0 - C_e)\mathrm{V}}{m}$$

where C_0 and C_t are the concentration of each pollutant in solution at initial and any time t, respectively. V is the volume of the solution and m is the mass of Janus micromotors used.

Supporting Information

Supporting Information is available from the Wiley Online Library or from the author.

Acknowledgements

This project received support from the Defense Threat Reduction Agency-Joint Science and Technology Office for Chemical and Biological Defense (Grant no. HDTRA1–13–1–0002). B. J-S acknowledges support from the People Programme (Marie Curie Actions) of the EU 7th Framework Programme (FP7 2007–2013) under REA Grant PIOF-GA-2012–326476. W. G. is a HHMI International Student Research fellow.

[1] W. F Paxton, K. C. Kistler, C. C. Olmeda, A. Sen, S. K. St. Angelo, Y. Cao, T. E. Mallouk, P. E. Lammert, V. H. Crespi, *J. Am. Chem. Soc.* **2004**, *126*, 13424.
[2] G. A. Ozin, I. Manners, S. Fournier-Bidoz, A. Arsenault, *Adv. Mater.* **2005**, *17*, 3011.
[3] J. Wang, *ACS Nano* **2009**, *3*, 4.
[4] J. Wang, *Nanomachines: Fundamentals and Applications*, Wiley-VCH, Weinheim, Germany, **2013**.
[5] W. Wang, W. Duan, S. Ahmed, T. E. Mallouk, A. Sen, *Nano Today* **2013**, *8*, 531.
[6] Y. Mei, A. A. Solovev, S. Sanchez, O. G. Schmidt, *Chem. Soc. Rev.* **2011**, *40*, 2109.
[7] T. Mirkovic, N. S. Zacharia, G. D. Scholes, G. A. Ozin, *ACS Nano* **2010**, *4*, 1782.
[8] P. Fischer, A. Ghosh, *Nanoscale* **2011**, *3*, 557.
[9] G. Huang, J. Wang, Y. Mei, *J. Mater. Chem.* **2012**, *22*, 6519.
[10] S. Sanchez, M. Pumera, *Chem.–Asian J.* **2009**, *4*, 1402.
[11] J. Wang, W. Gao, *ACS Nano* **2012**, *6*, 5745.
[12] L. K. E. A. Abdelmohsen, F. Peng, Y. Tu, D. A. Wilson, *J. Mater. Chem. B* **2014**, *2*, 2395.
[13] S. Sengupta, M. E. Ibele, A. Sen, *Angew. Chem. Int. Ed.* **2012**, *51*, 8434.
[14] W. Gao, J. Wang, *ACS Nano* **2014**, *8*, 3170.
[15] L. Soler, S. Sanchez, *Nanoscale* **2014**, *6*, 7175.
[16] L. Soler, V. Magdanz, V. M. Fomin, S. Sanchez, O. G. Schmidt, *ACS Nano* **2013**, *7*, 9611.
[17] T. H. Seah, G. Zhao, M. Pumera, *ChemPlusChem* **2013**, *78*, 395.
[18] J. Orozco, D. Vilela, G. Valdés-Ramírez, Y. Fedorak, A. Escarpa, R. Vazquez-Duhalt, J. Wang, *Chem. Eur. J.* **2014**, *20*, 2866.
[19] J. Orozco, G. Cheng, D. Vilela, S. Sattayasamitsathit, R. Vazquez-Duhalt, G. Valdés-Ramírez, O. S. Pak, A. Escarpa, C. Kan, J. Wang, *Angew. Chem. Int. Ed.* **2013**, *52*, 13276.
[20] M. Guix, J. Orozco, M. Garcia, W. Gao, S. Sattayasamitsathit, A. Merkoci, A. Escarpa, J. Wang, *ACS Nano* **2012**, *6*, 4445.
[21] W. Gao, X. Feng, A. Pei, Y. Gu, J. Li, J. Wang, *Nanoscale* **2013**, *5*, 4696.
[22] J. S. Mattson, H. B. Mark, Jr. *Activated Carbon: Surface Chemistry and Adsorption from Solution*, Marcel Dekker, New York, **1971**.
[23] Z. Yue, J. Economy, *J. Nanopart. Res.* **2005**, *7*, 477.

[24] *Activated Carbon Adsorption* (Ed: R. C. Bansal, M. Goyal), Taylor & Francis, Boca Raton, **2005**.
[25] *Activated Carbon Surfaces in Environmental Remediation* (Ed: T. J. Bandosz), Elsevier, The Netherlands, **2006**.
[26] I. Columbus, D. Waysbort, L. Shmueli, I. Nir, D. Kaplan, *Environ. Sci. Technol.* **2006**, *40*, 3952.
[27] K. Ohno, T. Minami, Y. Matsui, Y. Magara, *Water Res.* **2008**, *42*, 1753.
[28] R. Osovsky, D. Kaplan, H. Rotter, I. Nir, I. Columbus, *Ing. Eng, Chem. Res.* **2013**, *52*, 9705.
[29] K. Kadirvelu, C. Namasivayam, *Adv. Environ. Res.* **2003**, *7*, 471.
[30] J. Goel, K. Kadirvelu, C. Rajagopal, V. K. Garg, *J. Hazard. Mater. B* **2005**, *125*, 211.
[31] G. Loget, A. Kuhn, *J. Mater. Chem.* **2012**, *22*, 15457.
[32] S. Wang, N. Wu, *Langmuir* **2014**, *30*, 3477.
[33] J. Li, Z. Liu, G. Huang, Z. An, G. Chen, J. Zhang, M. Li, R. Liu, Y. Mei, *NPG Asia Mater.* **2014**, *6*, e94.
[34] W. Gao, A. Pei, R. Dong, J. Wang, *J. Am. Chem. Soc.* **2014**, *136*, 2276.
[35] W. Gao, S. Sattayasamitsathit, J. Orozco, J. Wang, *Nanoscale* **2013**, *5*, 8909.
[36] B. H. Hameed, A. T. M. Din, A. L. Ahmad, *J. Hazard. Mater.* **2007**, *141*, 819.

Received: July 24, 2014
Revised: August 15, 2014
Published online:

DOI: 10.1002/smll.201402215